Where Is the Needle Tip? VA Sensing Reveals Hidden Needle-Tissue Transitions During US Guidance

Robin Urrutia[1,2][0009−0003−9430−3474], Nazila Esmaeili[3][0000−0001−9741−9788], Axel Boese[4][0000−0002−5874−7145], Sasan Matinfar[5,6][0009−0003−6905−2001], Nikolaos Davaris[7][0000−0003−0283−9216], Christoph Arens[7][0000−0001−8072−1438], Christian Hansen[1,2][0009−0000−1530−4291], and Alfredo Illanes[1,2][0000−0002−0118−0483]

[1] Otto von Guericke University Magdeburg, Faculty of Computer Science, Virtual and Augmented Reality, Universitätsplatz 2, 39106 Magdeburg, Germany
robin.urrutia@ovgu.de
[2] Research Campus STIMULATE, Otto-Hahn-Str. 2, 39106 Magdeburg, Germany
[3] Center for Digital Surgery, Department of General, Visceral and Pediatric Surgery, University Medical Center Göttingen, 37075 Göttingen, Germany
[4] Otto von Guericke University Magdeburg, Innovation Laboratory for Image Guided Therapy, Leipziger Str. 44, 39120 Magdeburg, Germany
[5] Chair for Social Affective Touch, Technische Universität Dresden, 01069 Dresden, Germany
[6] Computer Aided Medical Procedures (CAMP), Technical University of Munich, 85748 Munich, Germany
[7] Department of Otorhinolaryngology, Head and Neck Surgery, and Plastic Surgery, Justus Liebig University of Giessen, 35392 Giessen, Germany

Abstract. Reliable identification of tissue transitions during ultrasound-guided needle insertion remains challenging, particularly when needle-tip visibility is degraded by imaging geometry or acoustic artifacts. Most prior work focuses on spatial localization, while fewer approaches address mechanically meaningful events such as boundary crossing between adjacent tissues. This study investigates whether proximal vibroacoustic (VA) sensing can detect tissue transitions during insertion. VA signals recorded at the needle hub were analyzed using a time–frequency representation, and statistical similarity to tissue-specific reference segments was quantified using the first-order Wasserstein distance. Transition time was derived from a log-distance ratio signal indicating regime change. Experiments were conducted on 42 controlled insertions in a layered ex-vivo biological phantom with synchronized ultrasound (US) video. Results show consistent regime shifts at tissue boundaries and temporal agreement with US-based annotations across different visibility conditions. These findings indicate that proximal VA sensing captures mechanical interaction changes associated with tissue transitions and may provide complementary feedback during US-guided procedures.

Keywords: Vibroacoustic · Ultrasound needle guidance · Needle tracking.

1 Introduction

Ultrasound-guided needle insertion is widely used in minimally invasive procedures such as biopsy, regional anesthesia, vascular access, and percutaneous therapy [6]. During these interventions, clinicians advance a needle toward a target under real-time ultrasound (US) imaging. Although US guidance is well established, accurate needle navigation remains technically demanding and strongly dependent on operator experience [9].

A critical moment during insertion is the crossing of a tissue boundary. As the needle traverses layered anatomical structures, it transitions between tissues with different mechanical properties [11, 7]. Correct identification of these transitions is important for maintaining orientation, avoiding unintended structures, and safely reaching the target. However, reliable visualization of the needle tip in US is not always possible [10]. Tip visibility depends on insertion angle, imaging conditions, and artifacts such as speckle or shadowing [12]. In out-of-plane insertions or low-contrast settings, the exact transition moment may not be clearly visible, increasing reliance on indirect visual cues and haptic perception [1].

Most technological solutions for needle guidance focus on spatial localization [3]. Image-based methods attempt needle detection or segmentation in US images but may degrade under challenging imaging conditions. External tracking systems, including electromagnetic or optical navigation, provide additional spatial information [5], yet require dedicated hardware, calibration, and workflow integration [3], increasing setup time and procedural complexity [13]. Instrumented needles with embedded force sensors have also been explored [4, 17]. While these approaches improve geometric tracking, they do not directly capture mechanical interaction changes occurring at tissue boundaries.

From a mechanical perspective, tissue transition involves altered interaction conditions at the needle tip [11]. Differences in stiffness and structure influence insertion dynamics and may generate vibrations that propagate along the needle shaft as structure-borne waves. These mechanically induced signals can be measured proximally, away from the contact point.

We refer to vibroacoustic (VA) sensing as the measurement of such signals at the needle hub, outside the patient's body. Because sensing occurs proximally, the distal needle geometry remains unmodified. The recorded signal reflects interaction dynamics and may provide information complementary to US imaging [8].

Previous studies have reported VA responses during needle insertion, demonstrating distinct signal patterns associated with structural transitions such as peritoneum puncture in cadaveric models, material changes in layered phantoms, and puncture or cavity events in layered synthetic phantoms [14, 15]. Beyond needle insertion, VA tissue–instrument interaction signals have also been used for biological tissue differentiation during computerized palpation [16]. However, prior work has not systematically analyzed tissue-to-tissue transition events during continuous US-guided needle insertion in biological tissues, nor evaluated temporally localized changes in proximal VA measurements under varying US

needle-tip visibility. It therefore remains unclear whether VA sensing can provide consistent information about boundary crossings during US-guided procedures.

In this work, we investigate proximal VA sensing as a complementary modality for tissue transition awareness during US-guided needle insertion. Synchronized US and VA recordings were acquired during controlled insertions into layered ex vivo tissues. A multiscale time–frequency representation and a regime-change detection framework were applied to identify transition points. The main contributions are twofold. First, we demonstrate that tissue-to-tissue transitions can be identified from proximal VA measurements, including cases with limited US needle-tip visibility. Second, we show that the VA signal exhibits stable intra-tissue regimes and distinct dynamical changes at boundary crossings. These findings support proximal VA sensing as a complementary perception channel and provide a foundation for interaction-based tissue characterization.

2 Methods

2.1 Experimental Setup and Data Acquisition

A total of 42 US-guided needle insertions were performed. Experiments were conducted using a multilayer phantom composed of two ex vivo biological tissues: bovine liver and chicken breast. The tissues were embedded in gelatin (Platinum Bloom 240) to provide structural support. The two tissue samples were positioned in direct contact with each other to create a defined tissue-to-tissue transition interface, allowing controlled insertion through consecutive biological layers. All insertions were performed using a 20G SPROTTE needle (Pajunk GmbH, Germany). VA signals generated during needle–tissue interaction were recorded using a proximal VA sensing module and acquisition system (SURAG Medical GmbH, Germany). The sensing module was connected directly to the needle hub via a standard luer-lock interface, without modification of the distal needle geometry (Fig. 1 - Components). The module communicated wirelessly via Bluetooth with a tablet computer (iPad, 10th generation), which served as the acquisition and storage unit of the system. Signals were visualized in real time and stored in WAV format at a sampling frequency of 16 kHz.

US imaging was performed using a B-mode system (GAMPT mbH, Germany) equipped with a 5 MHz linear probe. US videos were recorded at 60 frames per second. Synchronization between US and VA recordings was achieved by generating a common physical event visible in both modalities. At the beginning of each experiment, the needle was tapped three times against the US probe. These taps produced visible artifacts in the US image and corresponding peaks in the VA signal, enabling temporal alignment of both recordings.

From the recorded US videos, three time points were manually annotated: the time of first contact between the needle and the first ex vivo tissue (t_{entry}), the time of transition between the two biological tissues (t_{tc}), and the time at which the needle exited the second ex vivo tissue (t_{exit}). Annotations were performed frame-by-frame using the recorded US videos.

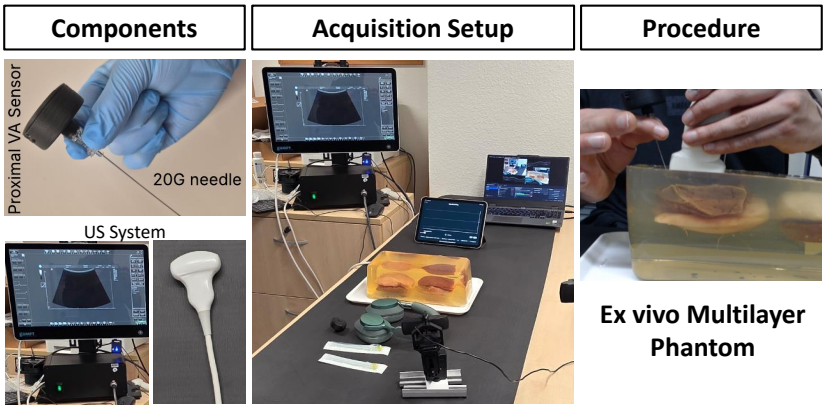

Fig. 1. Experimental setup for synchronized US and VA data acquisition, representing the components, acquisition setup, and procedure.

2.2 Data Processing

The data processing strategy is to take needle insertion procedure as a transition between two interaction regimes corresponding to the two tissue types. VA signals are transformed into a time–frequency representation, and an interaction-sensitive frequency band is extracted to compute a one-dimensional indicator. The statistical behavior of this indicator within each tissue is characterized using reference segments. To track regime evolution over time, a sliding window is compared to these references using the first-order Wasserstein distance, which quantifies differences between empirical signal distributions and measures similarity to each tissue-specific regime [2]. The resulting log-ratio signal reflects similarity to either regime and enables identification of the tissue transition. In parallel, US video data are processed independently to derive a motion-based visibility indicator. This allows evaluation of VA-based transition detection under varying levels of needle-tip visibility. A schematic overview of the complete workflow is shown in Fig. 2. The VA signals were first preprocessed to remove DC components and reduce background noise. The DC component was removed by subtracting the signal mean. Noise reduction was performed using spectral gating: the spectrogram was computed, a frequency-dependent noise threshold was estimated, and a binary spectral mask was applied to suppress components below this threshold, yielding a denoised signal. A continuous wavelet transform (CWT) with a Morlet mother wavelet was applied to obtain a time–frequency representation. From the CWT spectrum, a pseudo-frequency band showing strong dynamical variations during insertion was selected. The corresponding CWT coefficients were averaged across scales to derive the one-dimensional temporal indicator $I_{\mathrm{CWT}}(t)$.

Transition analysis was performed using a reference-based Wasserstein distance framework. For each recording, two reference segments were extracted from $I_{\mathrm{CWT}}(t)$. The first segment, denoted S_1, was selected within the interval

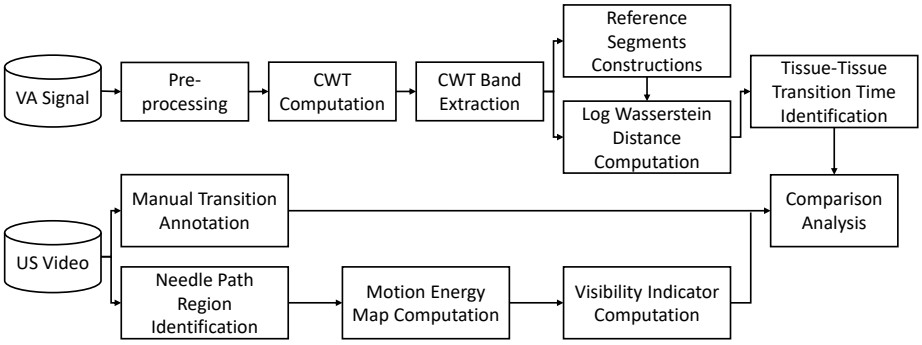

Fig. 2. Overview of the proposed processing framework.

$[t_{\text{entry}} + 100\,\text{ms},\ t_{\text{tc}} - 100\,\text{ms}]$, corresponding to insertion within the first tissue. The second segment, denoted S_2, was selected within $[t_{\text{tc}} + 100\,\text{ms},\ t_{\text{exit}} - 100\,\text{ms}]$, corresponding to insertion within the second tissue. Each segment had a duration of 300 ms. Prior to distance computation, segment values were normalized. A sliding window of 300 ms with 90% overlap was applied over $I_{\text{CWT}}(t)$. For each window $W(t)$, two first-order Wasserstein distances were computed as $D_1(t) = W\big(W(t), S_1\big)$ and $D_2(t) = W\big(W(t), S_2\big)$, where $W(\cdot,\cdot)$ denotes the Wasserstein distance between empirical distributions. A log-ratio signal was then defined as $R(t) = \log\left(\frac{D_1(t)}{D_2(t)}\right)$. Negative values of $R(t)$ indicate higher similarity to the first-tissue reference segment, while positive values indicate higher similarity to the second-tissue reference segment.

The transition time t^* was defined as the time instant at which $R(t)$ crossed zero with maximum slope in the vicinity of the regime change. For population-level analysis, each $R(t)$ signal was temporally aligned at t^* and normalized to the interval $[-1, 1]$ prior to averaging. To quantify agreement with US-based annotation, the absolute timing difference was computed as $|\Delta t| = |t^* - t_{\text{tc}}|$ for each insertion.

Needle-tip visibility was quantified independently from the US video using motion analysis along the insertion path. First, the needle path was defined by manually annotating the initial and final visible tip positions and constructing a central insertion axis between them. A corridor of ± 35 pixels around this axis was retained to account for slight needle bending, while regions outside the corridor were excluded. Within this corridor, a motion energy map was computed to capture temporal intensity changes along the insertion direction. The corridor was divided into 200 equally spaced patches along the axis. For each frame, squared frame-to-frame intensity differences were calculated within each patch, yielding a time-resolved spatial distribution of motion energy that highlights localized motion along the needle path. From this motion energy map, a visibility indicator was derived by extracting, for each frame, the maximum motion energy value across all patches.

When the needle tip is clearly visible and advancing, localized motion energy is concentrated along the axis, resulting in higher indicator values. When the tip is poorly visible, motion energy decreases and the indicator correspondingly drops. For each insertion, the median value of the visibility indicator over the insertion interval was used to assign the recording to one of three visibility groups (high, medium, or low) using empirically selected thresholds. These visibility groups were subsequently used to analyze the consistency of VA transition detection under varying levels of US visibility.

3 Results and Discussion

Figure 3 presents qualitative examples from three insertions with good, medium, and low needle-tip visibility in US. The three columns correspond to individual recordings, and the five rows show different signal representations. Row (a) displays the time–position motion energy map within the predefined needle corridor, and row (b) the corresponding visibility indicator. Row (c) shows the VA CWT spectrum, with dashed white lines marking the pseudo-frequency band used to compute the CWT-band indicator $I_{\mathrm{CWT}}(t)$ in row (d). Row (e) presents the log-ratio signal based on the Wasserstein distances to the two tissue reference segments. Green dashed lines indicate the US-based manual annotations t_{entry}, t_{tc}, and t_{exit}. Rows (a–b) demonstrate the variability of US visibility across recordings. In the good-visibility example, a clear diagonal motion-energy trace is visible throughout the insertion. In the medium-visibility case, the trace weakens around the expected transition region. In the low-visibility example, motion energy remains low across the entire insertion, indicating poor needle-tip visibility. Despite these differences, the VA analysis shows consistent behavior around the tissue transition.

The CWT spectra in row (c) indicate that the main excitation changes occur in the low pseudo-frequency range (5–120 Hz), used to compute $I_{\mathrm{CWT}}(t)$. The indicator in row (d) shows a clear change around t_{tc} in all cases. The log-ratio Wasserstein signal in row (e) reveals two distinct regimes separated by an abrupt change near t_{tc}, even when the transition is not clearly visible in US. Small temporal differences between the annotated t_{tc} and the detected time t^* (black dotted line) are expected under uncertain US-based tip annotation and are further analyzed in Fig. 3.

Figure 4 shows a population-level comparison of US visibility and VA regime behavior across all 42 insertions. The left heatmap presents the visibility indicator for each insertion, sorted from highest to lowest visibility, with time normalized between needle entry and exit. Visibility decreases from top to bottom, and several recordings show very low motion energy throughout. The right heatmap displays the corresponding log-ratio Wasserstein signals in the same order. Signals were temporally normalized and aligned so that the detected transition time t is centered at zero.

A clear regime separation is visible across all recordings, with negative values before and positive values after the transition. The sharpness and contrast

of this change remain comparable even in low-visibility cases, indicating that the VA regime transition is consistently identifiable independent of US visibility. Figure 5(b) presents the absolute timing difference $|\Delta t| = |t - t_{\mathrm{tc}}|$ between VA-based transition detection and US-based manual annotation, grouped by visibility level. Timing differences are smallest in high-visibility cases and increase for medium and low visibility, consistent with greater uncertainty in US annotation when the needle tip is poorly visible. Importantly, the VA regime change remains identifiable across all visibility levels (Fig. 5(a)), indicating a consistent change in interaction dynamics even when visual confirmation is limited.

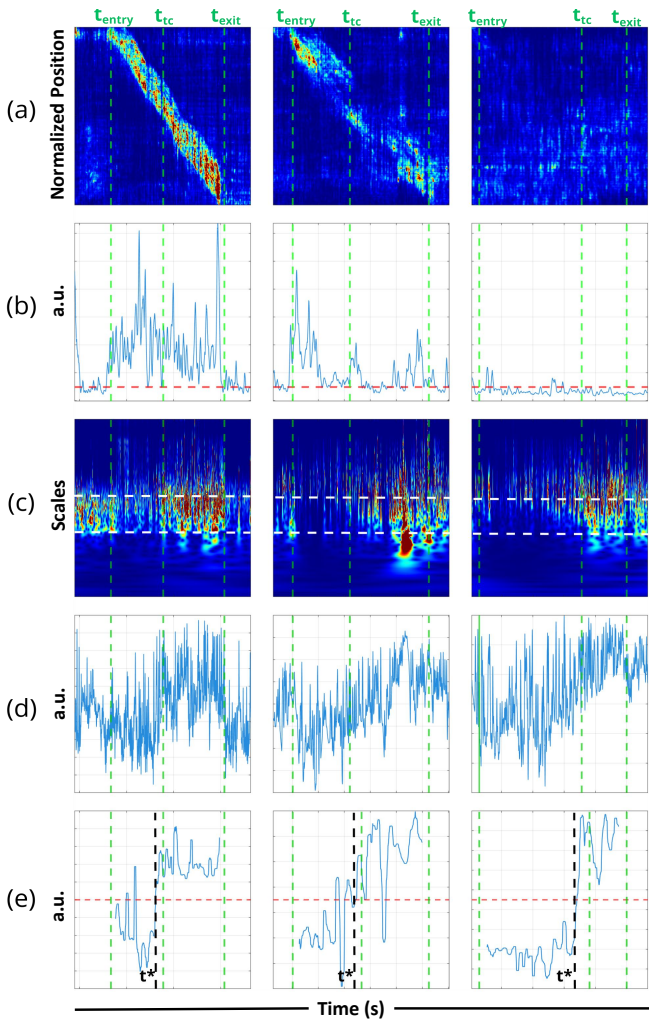

Fig. 3. Qualitative results of three US-guided insertions with good (left), medium (middle), and low (right) needle-tip visibility. Each row represents one indicator.

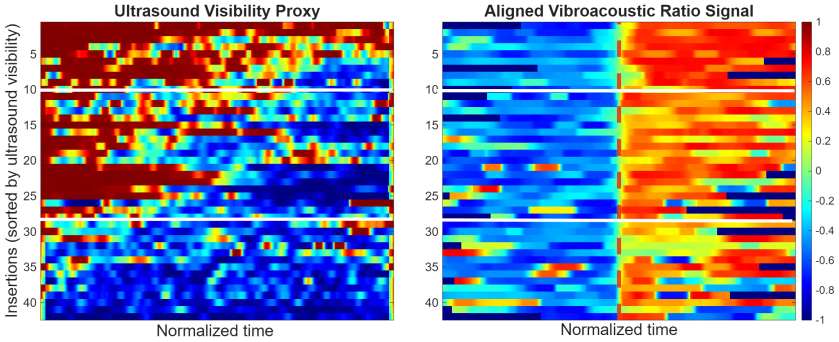

Fig. 4. Population-level comparison of US visibility and VA regime behavior. Left: visibility indicator. Right: corresponding log-ratio Wasserstein signals for the same insertions.

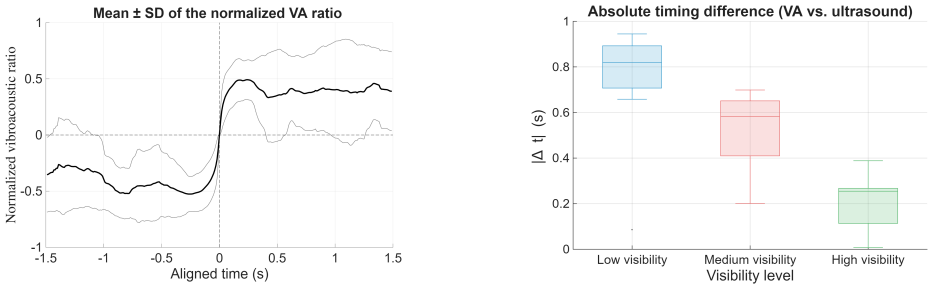

(a) (b)

Fig. 5. Timing agreement between VA transition detection and US-based annotation. (a): Signed timing difference across all insertions. (b): Absolute timing difference grouped by US visibility level (low, medium, and high).

4 Conclusions

This study investigated VA sensing as a complementary modality for tissue-transition awareness during US-guided needle insertion. By modeling the VA signal as a sequence of interaction regimes and quantifying distributional similarity using the Wasserstein distance, we showed that distinct dynamical behaviors occur in different tissue types. Tissue transitions were consistently reflected by abrupt regime changes in the log-ratio indicator. The VA regime change remained identifiable across varying US visibility levels. Although timing differences between VA detection and US annotation increased under low-visibility

conditions, this is consistent with greater uncertainty in manual tip identification. These findings indicate that proximal VA sensing provides mechanically derived transition information independent of visual contrast. Overall, VA measurements can augment needle guidance by providing complementary transition awareness when visual feedback is limited. Future work will focus on tighter integration of VA and US modalities. In particular, combining motion-energy analysis with VA regime indicators may allow compensation for visibility gaps and improved estimation of needle progression.

Acknowledgments. The work presented in this paper was funded by the European Regional Development Fund under operation number ZS/2023/12/182010, as part of the initiative "Sachsen-Anhalt WISSENSCHAFT Schwerpunkte" and was also supported by ANID (Chile) through its scholarship program Becas Chile/DAAD 2023-62230039. The authors would like to thank SURAG Medical GmbH for providing the vibroacoustic sensing system.

Disclosure of Interests. Nazila Esmaeili, Axel Boese and Alfredo Illanes are shareholders of SURAG Medical GmbH.

References

1. Arif, M., Moelker, A., van Walsum, T.: Needle tip visibility in 3d ultrasound images. Cardiovascular and Interventional Radiology **41**(1), 145–152 (2018). https://doi.org/10.1007/s00270-017-1798-7
2. Cazelles, E., Robert, A., Tobar, F.: The wasserstein-fourier distance for stationary time series. IEEE Transactions on Signal Processing **69**, 709–721 (2020). https://doi.org/10.1109/TSP.2020.3046227
3. Cheng, Z., Koskinopoulou, M., Bano, S., Stoyanov, D., Rajeeth Savarimuthu, T., Mattos, L.S.: Sensing technologies for guidance during needle-based interventions. IEEE Transactions on Instrumentation and Measurement **73**, 1–15 (2024). https://doi.org/10.1109/TIM.2024.3441017
4. Elayaperumal, S., Bae, J.H., Daniel, B.L., Cutkosky, M.R.: Detection of membrane puncture with haptic feedback using a tip-force sensing needle. In: 2014 IEEE/RSJ International Conference on Intelligent Robots and Systems. pp. 3975–3981. IEEE (2014). https://doi.org/10.1109/IROS.2014.6943121
5. Franz, A.M., Haidegger, T., Birkfellner, W., Cleary, K., Peters, T.M., Maier-Hein, L.: Electromagnetic tracking in medicine—a review of technology, validation, and applications. IEEE transactions on medical imaging **33**(8), 1702–1725 (2014). https://doi.org/10.1109/TMI.2014.2321777
6. Fukui, S., Rokutanda, R., Kawaai, S., Suda, M., Iwata, F., Okada, M., Kishimoto, M.: Current evidence and practical knowledge for ultrasound-guided procedures in rheumatology: Joint aspiration, injection, and other applications. Best Practice & Research Clinical Rheumatology **37**(1), 101832 (2023). https://doi.org/10.1016/j.berh.2023.101832
7. van Gerwen, D.J., Dankelman, J., van den Dobbelsteen, J.J.: Needle–tissue interaction forces–a survey of experimental data. Medical engineering & physics **34**(6), 665–680 (2012). https://doi.org/10.1016/j.medengphy.2012.04.007

8. Illanes, A., Boese, A., Maldonado, I., et al.: Novel clinical device tracking and tissue event characterization using proximally placed audio signal acquisition and processing. Scientific Reports **8**, 1–11 (2018). https://doi.org/10.1038/s41598-018-30641-0
9. Marhofer, P., Chan, V.W.: Ultrasound-guided regional anesthesia: current concepts and future trends. Anesthesia & Analgesia **104**(5), 1265–1269 (2007). https://doi.org/10.1213/01.ane.0000260614.32794.7b
10. Neal, J.M.: Ultrasound-guided regional anesthesia and patient safety: update of an evidence-based analysis. Regional Anesthesia & Pain Medicine **41**(2), 195–204 (2016). https://doi.org/10.1097/AAP.0000000000000295
11. Okamura, A.M., Simone, C., O'leary, M.D.: Force modeling for needle insertion into soft tissue. IEEE transactions on biomedical engineering **51**(10), 1707–1716 (2004). https://doi.org/10.1109/TBME.2004.831542
12. Quien, M.M., Saric, M.: Ultrasound imaging artifacts: How to recognize them and how to avoid them. Echocardiography **35**(9), 1388–1401 (2018). https://doi.org/10.1111/echo.14116
13. Scholten, H.J., Pourtaherian, A., Mihajlovic, N., Korsten, H.H., A. Bouwman, R.: Improving needle tip identification during ultrasound-guided procedures in anaesthetic practice. Anaesthesia **72**(7), 889–904 (2017). https://doi.org/10.1111/anae.13921
14. Spiller, M., Esmaeili, N., Sühn, T., Boese, A., Turial, S., Gumbs, A.A., Croner, R., Friebe, M., Illanes, A.: Enhancing veress needle entry with proximal vibroacoustic sensing for automatic identification of peritoneum puncture. Diagnostics **14**(15), 1698 (2024). https://doi.org/10.3390/diagnostics14151698
15. Steeg, K., Serwatka, W., Rzepka, D., Oran, H., Özdil, O., Heryan, K., Krombach, G., Friebe, M.: Vibroacoustic signatures: proof of concept for simple material characterization during needle interventions. International Journal of Computer Assisted Radiology and Surgery **20**(9), 1807–1815 (2025). https://doi.org/10.1007/s11548-025-03492-0
16. Sühn, T., Esmaeili, N., Spiller, M., Costa, M., Boese, A., Bertrand, J., Pandey, A., Lohmann, C., Friebe, M., Illanes, A.: Vibro-acoustic sensing of tissue-instrument-interactions allows a differentiation of biological tissue in computerised palpation. Computers in Biology and Medicine **164**, 107272 (2023). https://doi.org/10.1016/j.compbiomed.2023.107272
17. Trejos, A., Patel, R., Naish, M.: Force sensing and its application in minimally invasive surgery and therapy: a survey. Proceedings of the Institution of Mechanical Engineers, Part C: Journal of Mechanical Engineering Science **224**(7), 1435–1454 (2010). https://doi.org/10.1243/09544062JMES1917